High performance piezotronic spin transistors using molybdenum disulfide nanoribbon

Journal Pre-proof

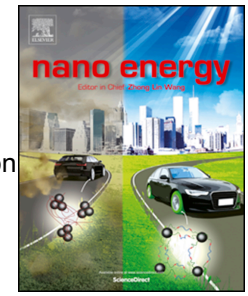

High performance piezotronic spin transistors using molybdenum disulfide nanoribbon

X.F. Yan, Q. Chen, L.L. Li, H.Z. Guo, J.Z. Peng, F.M. Peeters

PII: S2211-2855(20)30510-3

DOI: https://doi.org/10.1016/j.nanoen.2020.104953

Reference: NANOEN 104953

To appear in: *Nano Energy*

Received Date: 6 April 2020

Revised Date: 7 May 2020

Accepted Date: 10 May 2020

Please cite this article as: X.F. Yan, Q. Chen, L.L. Li, H.Z. Guo, J.Z. Peng, F.M. Peeters, High performance piezotronic spin transistors using molybdenum disulfide nanoribbon, *Nano Energy* (2020), doi: https://doi.org/10.1016/j.nanoen.2020.104953.

Credit Author Statement

X. F. Yan: Methodology, Formal analysis, Writing- Original draft preparation; **Q. Chen:** Supervision, Conceptualization, Formal analysis, Validation, Writing- Original draft preparation; Writing- Reviewing and Editing**; L. L. Li:** Formal analysis, Writing- Reviewing and Editing; **H. Z. Guo:** Validation, Formal analysis; **J. Z. Peng:** Validation, Formal analysis; **F. M. Peeters:** Writing- Reviewing and Editing

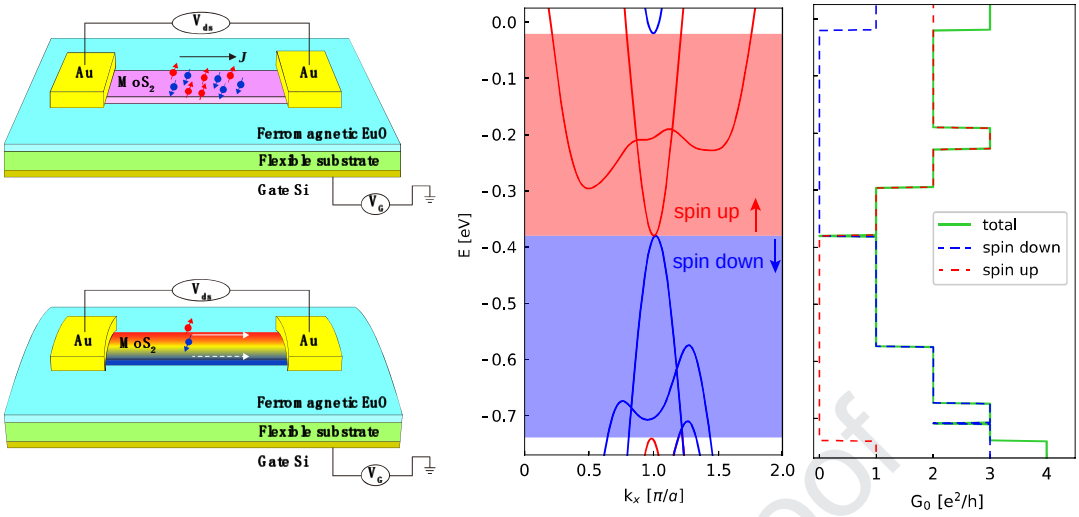

Due to the strong piezoelectric property of monolayer MoS_2, strain applied along the zigzag direction can generate a piezoelectric field along the armchair direction. The edge states can be separated by the piezoelectric field. By applying an exchange field produced from a ferromagnetic insulator material, spin polarization is found to be effectively controlled by strain. For both spin up and spin down states, their polarization intensity can be tuned up to 100% over a wide modulating region.

High Performance Piezotronic Spin Transistors using Molybdenum Disulfide Nanoribbon

X. F. Yan[1,2], Q. Chen[2,*], L. L. Li[3,4,†], H. Z. Guo[5], J. Z. Peng[1],

and F. M. Peeters[6,3,§]

1 *College of Physics and Mechanical & Electrical Engineering, Jishou University, Jishou 416000, China*

2 *School of Computational Science and Electronics, Hunan Institute of Engineering, Xiangtan 411104, China*

3 *Department of Physics, University of Antwerp, Groenenborgerlaan 171, B-2020 Antwerp, Belgium*

4 *Department of Physics, University of Duisburg-Essen, Lotharstr. 1, 47057 Duisburg, Germany*

5 *College of Physics, Sichuan University, Chengdu 610064, China*

6 *School of Physics and Astronomy and Yunnan Key Laboratory for Quantum Information, Yunnan University, Kunming 650091, China*

* cqhy1127@aliyun.com

† longlong.li@uni-due.de

§ francois.peeters@uantwerpen.be

Abstract: Two-dimensional (2D) materials are promising candidates for atomic-scale piezotronics and piezophototronics. Quantum edge states show fascinating fundamental physics such as nontrivial topological behavior and hold promising practical applications for low-power electronic devices. Here, using the tight-binding approach and quantum transport simulations, we investigate the piezotronic effect on the spin polarization of edge states in a zigzag-terminated monolayer MoS_2 nanoribbon. We find that the strain-induced piezoelectric potential induces a phase transition of edge states from metal to semiconductor. However, in the presence of exchange field, edge states become semi-metallic with significant spin splitting and polarization that can be tuned by external strain. We show that quantum transport

conductance exhibits a 100% spin polarization over a wide range of strain magnitudes. This effect is used in a propose prototype of piezotronic spin transistor. Our results provide a fundamental understanding of the piezotronic effect on edge states in zigzag monolayer MoS_2 nanoribbons and are relevant for designing high-performance piezotronic spin devices.

Keywords: Piezoelectric property, MoS_2 nanoribbon, Spin transistors, Edge states.

I. INTRODUCTION

Monolayers of transition metal dichalcogenides (TMDs), as an important class of two-dimensional (2D) semiconducting materials, have drawn a lot of interest in both fundamental research and practical applications [1, 2]. Compared with gapless graphene, the TMD family of materials exhibit many advantages in the realm of optoelectronic device designs due to their wide direct-bandgap, high transparency and good mechanical flexibility. The tunable bandgap by altering layers or applying mechanical strain makes TMD materials operate over a wide range of wavelengths that is important for photoelectric detection [3]. Due to the coupling of strong piezoelectric and semiconducting properties, TMDs turn out to be important for potential applications in electromechanical transducers and energy harvestings, such as nanogenerators and solar cells [4, 5].

Spin, associated with the magnetic moment of the electron, serve as an internal quantum degree of freedom that is promising for magnetic information storage and future electronics [6]. Although TMDs is a nonmagnetic material, it has also widespread applications in spintronics because of the presence of strong intrinsic spin-orbit coupling (SOC) (0.15 eV for MoS_2 and 0.46 eV for WSe_2) [7]. Many spin-relevant physical phenomena in TMDs have been extensively explored including valley pseudospin [8], quantum spin Hall insulator [9], semimetallicity and metallicity. By breaking spatial reversal symmetry, an electric field will act as a versatile control parameter for SOC [10].

Following the rapid development of various nanogenerators, piezotronic and piezo-phototronic starts to become appealing for many high performance electronic and photoelectronic applications. The primary material groups for those devices are piezoelectric semiconductors including conventional three-dimensional (3D) bulk materials such as ZnO,

GaN and CdS, and some 2D materials such as MoS_2 and *h*-BN [11, 12]. Based on those 3D and 2D materials, Wang et. al. have developed and fabricated a large number of high performance electro-chemical devices ranging from nanogenerator [13, 14] and field effect transistor [15] to strain sensor array [16] and optical sensor integration [17]. Zhang et. al. has demonstrated that the basic mechanism of piezotronic effect is to exploit mechanical strain-generated polarization field to control electron and hole behaviors in nanomaterials [18]. Moreover, a strain-controlled power device (SPD) was designed by using an AlGaN/AIN/GaN heterojunction, which uses external strain to modulate the output power by emulating the human reflex process [19]. More recently, piezotronic effect on quantum materials has been reviewed in particular for spin-related characteristics [20]. Piezotronic effect on topological insulators have been extensively studied for several material systems, such as HgTe/CdTe and GaN/InN quantum well [21, 22], for which large SOC is a prerequisite for a topological phase transition. Zhu et. al. have also reported that a piezoelectric field can tune Rashba-type SOC at ZnO/P_3HT interface at room temperature, paving the way for promising potential spintronic applications based on the piezotronic effect [23]. Quantum states can be tuned by the Piezotronic effect, which is crucial for developing quantum-related piezotronics. Unfortunately, the existing investigations are very limited especially for spin-related electronic transport [20].

Here, we theoretically investigate spin transport by edge-states in a zigzag MoS_2 nanoribbon under uniaxial strain and an exchange field. Due to the strong piezoelectric property of monolayer MoS_2, strain applied along the zigzag direction can generate a piezoelectric field along the armchair direction. This piezoelectric field can open a gap in the edge state spectrum, leading to a metal-to-semiconductor phase transition. By applying an exchange field produced from a ferromagnetic insulator material [24-26], spin polarization is found to be effectively controlled by strain. For both spin up and spin down states, their polarization intensity can be tuned up to 100% over a wide modulating region. By performing quantum transport calculations, we examine polarization conductance, polarization ratio and electronic density distribution.

II. THEORY AND MODEL

The studied system is schematically shown in Fig. 1(a) with a zigzag molybdenum disulfide nanoribbon (ZMDSN) connected to two leads that act as electrodes. Generally, monolayer MoS_2 nanoribbon has two types of boundary atomic arrangements, i.e., armchair and zigzag. Here, we focus on zigzag boundaries because its edge states exhibit spin polarization. Due to strong piezoelectric property of monolayer MoS_2, a polarized field can be induced by external strain, as shown in Figs. 1(b) - (d). For tensile strain applied perpendicular to the zigzag boundary, the induced polarization field is pointed from S-terminal to Mo-terminal, i.e., inverse *y*-axis direction. For compressive strain, the polarization field is along *y*-axis direction. Such polarization field can change the electronic properties of MoS_2 ribbon, especially for edge-state electrons as studied below.

The low-energy electronic properties of a monolayer MoS_2 can well be described by the multi-band Slater-Koster tight-binding (TB) model obtained from first principles calculations [27-30]. This TB model is based on six reduced atomic orbitals as the basis set which consist of $\left(d_{z^2}, d_{x^2-y^2}, d_{xy}\right)$ for Mo atoms and $\left[\frac{1}{\sqrt{2}}\left(p_x^t + p_x^b\right), \frac{1}{\sqrt{2}}\left(p_y^t + p_y^b\right), \frac{1}{\sqrt{2}}\left(p_z^t - p_z^b\right)\right]$ for S atoms, where *t* and *b* refer to the top and bottom S layers, respectively. Within this basis set, the TB Hamiltonian is written as [31, 32]

$$H = \sum_{i,\mu}\left(\varepsilon_{i,\mu}^{M} c_{i,\mu}^{\dagger} c_{i,\mu} + \varepsilon_{i,\mu}^{S} b_{i,\mu}^{\dagger} b_{i,\mu}\right) + \sum_{<<ij>>,\mu\nu}\left(t_{ij,\mu\nu}^{MM} c_{i,\mu}^{\dagger} c_{j,\nu} + t_{ij,\mu\nu}^{SS} b_{i,\mu}^{\dagger} b_{j,\nu}\right) + \sum_{<ij>,\mu\nu} t_{ij,\mu\nu}^{MS} c_{i,\mu}^{\dagger} b_{j,\nu} + H.c. \quad (1)$$

where i, j and μ, ν run over the lattice sites and atomic orbits, respectively. $c_{i,\mu}^{\dagger}$ and $c_{i,\mu}$ ($b_{i,\mu}^{\dagger}$ and $b_{i,\mu}$) represent the creation and annihilation operators for electrons on Mo (S) atoms. All Slater-Koster hopping parameters $t_{ij,\mu\nu}^{MM}$, $t_{ij,\mu\nu}^{SS}$ and $t_{ij,\mu\nu}^{MS}$ are given in Ref. [31]. In this work, we focus on spin-polarized edge states of a monolayer MoS2 ribbon, which are located in the low-energy region (i.e. within the bulk gap of the ribbon) and therefore can be described well by this six-band TB model. Similar to Ref. [32], an exchange field is also applied to produce spin splitting. The on-site energies of Mo and S atoms are given by

$$\varepsilon_i^M = \begin{bmatrix} \Delta_0 & 0 & 0 \\ 0 & \Delta_2 & -is\lambda_M \\ 0 & is\Delta_M & \Delta_2 \end{bmatrix} - hs\mathbf{I} \tag{2}$$

and

$$\varepsilon_i^S = \begin{bmatrix} \Delta_p + t_{xx}^{\perp} & -\frac{1}{2}is\lambda_S & 0 \\ \frac{1}{2}is\lambda_S & \Delta_p + t_{yy}^{\perp} & 0 \\ 0 & 0 & \Delta_z - t_{zz}^{\perp} \end{bmatrix} - hs\mathbf{I} \tag{3}$$

where h refers to the strength of the exchange field. λ_M and λ_S represent the SOC strengths of the Mo and S atoms [33], respectively. **I** is the identity matrix, and s refers to the spin angular momentum along the z-axis. The corresponding parameters are given in Table I.

Table □: On-site energies of the tight-binding parameters in monolayer MoS_2 (in eV) [34]

Symbol	Value	Symbol	Value
Δ_0	-1.094	Δ_2	-1.512
Δ_p	-3.560	Δ_z	-6.886
λ_M	0.075	λ_S	0.052
$t_{xx(yy)}^{\perp}$	-0.467	$t_{zz}^{\perp}$	1.225

When strain is applied, the TB parameters are changed due to the variation in atomic bond lengths. It was shown in recent work [34] that the effect of strain is considered by modifying the hopping energy as

$$t_{ij,\mu\nu}\left(\mathbf{r}_{ij}\right) = t_{ij,\mu\nu}\left(\mathbf{r}_{ij}^0\right)\left(1 - \Lambda_{ij,\mu\nu}\frac{\left|\mathbf{r}_{ij} - \mathbf{r}_{ij}^0\right|}{\left|\mathbf{r}_{ij}^0\right|}\right) \tag{4}$$

where $\left|\mathbf{r}_{ij}^0\right|$ is the distance between i atom and j atom without strain, and $\left|\mathbf{r}_{ij}\right|$ refers to the distance in the presence of strain. $\Lambda_{ij,\mu\nu}$ is the dimensionless bond-resolved local electron-

phonon coupling. Following the Wills-Harrison argument, $\Lambda_{ij,S-S}$ = 3, $\Lambda_{ij,Mo-S}$ = 4, and $\Lambda_{ij,Mo-Mo}$ = 5 [34, 35]. The variation of bond length has no influence on the on-site energy. The other parameters can be found in Ref. [34].

In addition, when tensile or compressive strain is applied along the armchair edge, a potential is produced across the monolayer MoS_2 nanoribbon due to the piezoelectric effect. Various studies obtained the dependence of the polarization potential on the applied strain [36, 37]. Here, we give an explicit piezoelectric potential which is written as

$$V_{piezo} = \frac{e_{11}\varepsilon}{2\pi\varepsilon_0\varepsilon_r}\ln\left(\frac{y}{W-y}\right) \tag{5}$$

where e_{11} = 3.06 × 10^{-10} C/m is the clamped-ion piezoelectric coefficient [38], ε_0 = 8.85 × 10^{-12} F/m and ε_r = 3.3 refer to vacuum dielectric constant and relative dielectric constant of MoS_2, respectively. ε is the applied strain, W is the nanoribbon width, and y is the coordinate along the armchair direction shown in Fig. 1(a).

We employ the quantum transport software packages *Kwant* and *Pybinding* to obtain numerical results for the conductance [39, 40]. To measure the degree of spin polarization in the electronic transport, we also calculate the ratio $p = \frac{G_\uparrow - G_\downarrow}{G_\uparrow + G_\downarrow}$ [32].

III. RESULTS AND DISCUSSIONS

To calculate the spin polarized transport by edge states, we introduce a two-terminal device based on a zigzag monolayer MoS_2 nanoribbon in the presence of uniaxial strain, as shown in Fig. 1. The number of atomic layer N along y axis is used to describe the width of the nanoribbon. The electronic properties of MoS_2 nanoribbon depend sensitively on their edge structure due to the different constituent atoms located at opposite edges. Band dispersions of a 21-ZMDSN (N=21 stands for the number of atomic layer) is depicted in Fig. 2. In the absence of external strain, the dispersion spectrum has two obvious band curves that intersect each other. Those two curves are edge states with the electrons located at the boundaries. Band intersection indicates the metallicity of edge states. Because strain-induced

piezoelectric charges also reside on the boundaries, edge-states electrons will be modulated by external strain, as shown in Figs. 2(b) and (c). When the strain is applied, a piezoelectric field is induced across the ZMDSN, and its direction is determined by the type of strain. As shown in Figs. 1(b) and (d), the direction of piezoelectric field under tensile strain is along *-y* axis, and it is along the opposite direction for compressive strain. The directional difference is expected to result in different band dispersions and electronic behaviors due to dissimilarity in the chemical nature of the opposite edges. Fig. 2(b) shows that under compressive strain, the edge states intersect more strongly, and consequently, the corresponding inverted (negative) gap becomes large, leading to stronger metallic feature. However, in the presence of tensile strain edge states can be separated by a positive gap, as shown in Fig. 2(c). In this case, ZMDSN becomes semiconducting due to the gapped edge states. The change from metallic to semiconducting by strain is mainly due to the strain-induced piezoelectric field. However, the edge states under strain are still spin degenerate.

It is known that the nonlocal exchange field generated by the ferromagnetic substrate breaks time reversal symmetry, which can lift the degeneracy between spin-up and spin-down bands. Although there is a large spin splitting by the exchange field, no energy gap can be opened between two successive subbands with the same spin. Therefore, spin polarization cannot be realized by only the exchange field. However, this will be changed when an exchange field is combined with tensile strain. Fig. 3 shows the band structure of 21-ZMDSN under fixed strain (6.9%) where the spin-up subband of the lowest conduction band exactly touches the spin-down subband of the highest valence band at a critical energy of -0.383 eV. As can be seen, the energy regions corresponding to the spin-up and spin-down subbands, as shaded by different colors in Fig. 3(a), are well separated beyond this critical energy. This indicates that by tuning the Fermi level within these two energy regions, excellent spin polarization can be achieved. In an experiment, the Fermi level can be tuned by means of doping or by a split gate voltage [41, 42]. To demonstrate such spin polarization, spin-dependent transport conductance and spin polarization ratio were calculated and the corresponding results are shown in Figs. 3(b) and 3(c), respectively. It is shown that the spin-up conductance vanishes in the energy region from -0.738 to -0.383 eV, thereby leading to a

100% spin down polarization. On the contrary, spin-up electrons dominate transport when the Fermi level is located within the energy region of -0.383 ~ -0.017 eV. Outside those two polarized regions, transport is led by both spin-up and spin-down states reducing the spin polarization ratio below 1 (i.e., electronic transport is not perfectly spin polarized).

Table. II shows the critical exchange field strengths and the induced spin gaps for different values of the strain. As can be seen, both the strength of the critical field and the size of the induced spin gap $\boldsymbol{\Delta_s}$ also increase with the magnitude of strain. The reason is that the strain induced gap increase with the strain as shown in Fig. 2(c). Thus, spin splitting of edge states caused by the exchange field can occur in a larger energy region.

Table II: The critical exchange field and the induced spin gap for half-metallic states under different strain.

ε / %	h/λ_M	$\Delta s\,(\mathrm{meV})$
4	0.31	□46
5	1.02	□154
6	1.75	□262
7	2.47	□369

In order to further demonstrate the effect of strain-induced piezoelectric field on spin polarized transport, Fig. 4 gives the energy spectrum and spin polarization under uniform piezoelectric field, which is written as $\boldsymbol{E_{piezo}} = \dfrac{\boldsymbol{e_{11}\varepsilon}}{\boldsymbol{\varepsilon_0\varepsilon_r W}}$. By taking the spatial gradient of the nonuniform piezoelectric potential [Eq. (5)], we found that the corresponding piezoelectric field has the largest (smallest) amplitude at the boundaries (interior) of the ribbon. This directly leads to a significant spin polarization induced by edge states, as expected. Now the piezoelectric field is a constant and thus has equal amplitudes both at the edges and the center. Moreover, this uniform piezoelectric field at the boundaries is smaller than the nonuniform piezoelectric field given by Eq. (5). Therefore, the spin induced gap Δs decreases for uniform piezoelectric field. Additionally, the spin induced gap Δ_s is almost constant for exchange field $\boldsymbol{h} > 1.075\lambda_M$ ($\boldsymbol{h}$=1.075λ_M is the critical exchange field for half-metallic states under strain 6.9%) under uniform piezoelectric field.

Fig. 5 plots the contour map of spin polarization as a function of strain and Fermi level at fixed exchange field $(h=1.075\lambda_M)$. As can be seen, full spin polarization cannot be realized when the magnitude of tensile strain is less than 3.6%. This is because the low piezoelectric field at small strain is not sufficient to trigger a complete separation of spin subbands. In this case, both the spin-up and spin-down states contribute to transport at a fixed Fermi level, and thus the conductance is composed of these two spin contributions. As the magnitude of tensile strain increases beyond a critical value $(\varepsilon_1 > 3.6\%)$, the subbands with different spin are well separated, and fully spin polarization emerges in the two energy regions indicated by red and green colors and its sign can be switched between -1 and 1 by tuning the Fermi energy. Another critical strain is $\varepsilon_2=6.9\%$, for which the conduction and valence bands are not inverted but instead touch each other [seeing Fig. 3(a)]. It is an ideal situation for full spin polarization. Further increasing strain from 6.9% to 8.9% shows a zero polarization region where the Fermi level is located in the band gap. In this case, the conductance is zero at zero temperature. Therefore, edge states exhibit semiconducting property. When strain is larger than 8.9%, there is a gap between two fully polarization ranges of spin up and spin down states.

In Fig. 6, we show the electronic band dispersion and density distribution of 21-ZMDSN at Fermi energy -0.4 eV under three different strains: 6.6%, 7.6% and 8.6%, as labeled by *A*, *B* and *C* in Fig. 5. When strain is set to 6.6%, the ribbon exhibits a semi-metallic phase due to the gapless edge states. In this phase, the conduction-band minimum and valence-band maximum correspond to different spin states and the electronic spectrum has zero band gap. It was shown that in the semi-metallic phase spin polarization can be realized by changing the Femi energy [32]. For example, only valence-band spin-down band intersects at the Fermi level of -0.4 eV, leading to a fully spin down polarization. The left of Fig. 6(d) shows electronic density distribution with this full polarization, and only spin down electrons can travel through the ribbon along the Mo boundary. By increasing strain to 7.6%, this ribbon becomes semiconducting where no states are found at the Fermi level of -0.4 eV, as shown in Fig. 6(b). Further increasing the strain to 8.6%, the situation becomes distinctively different:

only spin-up electrons emerge in the ribbon, leading to a fully spin-up polarization. Its electronic density distribution is shown in the right of Fig. 6(d).

The key idea of strain modulated spin polarization is to utilize a piezoelectric field to control the edge states of zigzag monolayer MoS_2 nanoribbon, which is a direct consequence of the piezotronic effect. Based on this modulation, a high-performance piezotronic spin transistor can be designed. Recent experiments reported that edge states in MoS_2 systems are favorable to realize such type of devices [43]. Fig. 7 depicts the schematic diagram of such spin transistor in an experimental set-up. A ferromagnetic insulator placed on a flexible substrate is used to provide an exchange field. Ferromagnetic material EuO or EuS is deposited on monolayer MoS_2 by reactive molecular beam epitaxy, which has been successfully applied on graphene for the realization of exchange proximity coupling [24]. Polyethylene terephthalate is very commonly used as a flexible substrate for MoS_2 flakes [4]. When no strain is applied, spin polarization is zero, as shown in Fig. 7(a). By mechanically bending the flexible substrate, a tensile strain can be applied on the MoS_2 ribbon. Strain-induced piezoelectric field enhances the spin polarization of edge-state electrons, giving rise to pure spin current flowing through the MoS_2 ribbon in Fig. 7(b).

IV. SUMMARY

We have theoretically studied the impact of the piezotronic effect on spin-dependent transport of the edge states in a two-terminal monolayer MoS_2 nanoribbon with zigzag boundaries. We calculated the band dispersion, spin-dependent conductance, electronic density distribution and spin polarization in the absence and presence of external strain. We found that monolayer MoS_2 nanoribbon presents semiconducting or metallic properties depending on the piezoelectric potential induced by strain. By using a combination of external strain with an exchange field one can control the spin polarization of edge states. We showed that a 100% spin-polarized conductance is achieved both for spin-up and spin-down edge states. Our calculations offer a method for designing high performance piezotronic spin transistors.

Acknowledgements

This work was supported by Hunan Provincial Natural Science Foundation of China (Nos. 20 15JJ2040, 2018JJ2078), Scientific Research Fund of Hunan Provincial Education Department (19A106), and the Flemish Science Foundation (FWO-VI).

Reference

[1] X. Duan, C. Wang, A. Pan, R. Yu, X. Duan, Two-dimensional transition metal dichalcogenides as atomically thin semiconductors: opportunities and challenges, Chem. Soc. Rev., 44 (2015) 8859-8876.
[2] S. Manzeli, D. Ovchinnikov, D. Pasquier, O. V. Yazyev, A. Kis, 2D transition metal dichalcogenides, Nat Rev Mater, 2 (2017) 17033.
[3] F. Xia, H. Wang, D. Xiao, M. Dubey, A. Ramasubramaniam, Two-dimensional material nanophotonics, Nature Photon, 8 (2014) 899-907.
[4] W. Wu, L. Wang, Y. Li, F. Zhang, L. Lin, S. Niu, D. Chenet, X. Zhang, Y. Hao, T. F. Heinz, J. Hone, Z. L. Wang, Piezoelectricity of single-atomic-layer MoS_2 for energy conversion and piezotronics, Nature, 514 (2014) 470-474.
[5] M. L. Tsai, S. H. Su, J. K. Chang, D. S. Tsai, C. H. Chen, C. I. Wu, L. J. Li, L. J. Chen, J. H. He, Monolayer MoS_2 Heterojunction Solar Cells, ACS Nano, 8 (2014) 8317-8322.
[6] S. A. Wolf, D. D. Awschalom, R. A. Buhrman, J. M. Daughton, S. von Molnar, M. L. Roukes, A. Y. Chtchelkanova, D. M. Treger, Spintronics: A Spin-Based Electronics Vision for the Future, Science, 294 (2001) 1488-1495.
[7] Z. Y. Zhu, Y. C. Cheng, U. Schwingenschlögl, Giant spin-orbit-induced spin splitting in two-dimensional transition-metal dichalcogenide semiconductors, Phys. Rev. B, 84 (2011) 153402.
[8] X. Xu, W. Yao, D. Xiao, T. F. Heinz, Spin and pseudospins in layered transition metal dichalcogenides, Nature Phys, 10 (2014) 343-350.
[9] X. Qian, J. Liu, L. Fu, J. Li, Quantum spin Hall effect in two-dimensional transition metal dichalcogenides, Science, 346 (2014) 1344-1347.
[10] T. Jungwirth, J. Wunderlich, K. Olejnik, Spin Hall effect devices, Nature Mater, 11 (2012) 382-390.
[11] Y. Peng, M. Que, J. Tao, X. Wang, J. Lu, G. Hu, B. Wan, Q. Xu, C. Pan, Progress in piezotronic and piezo-phototronic effect of 2D materials, 2D Materials, 5 (2018) 042003.
[12] Z. L. Wang, W. Wu, C. Falconi, Piezotronics and piezo-phototronics with third-generation semiconductors, MRS Bull., 43 (2018) 922-927.
[13] Y. Qin, X. Wang, Z. L. Wang, Microfibre–nanowire hybrid structure for energy scavenging, Nature, 451 (2008) 809-813.
[14] Z. L. Wang, J. Song, Piezoelectric nanogenerators based on zinc oxide nanowire arrays, Science, 312 (2006) 242-246.
[15] X. Wang, J. Zhou, J. Song, J. Liu, N. Xu, Z. L. Wang, Piezoelectric field effect transistor and nanoforce sensor based on a single ZnO nanowire, Nano Lett., 6 (2006) 2768-2772.
[16] J. Zhou, Y. Gu, P. Fei, W. Mai, Y. Gao, R. Yang, G. Bao, Z. L. Wang, Flexible Piezotronic

Strain Sensor, Nano Lett., 8 (2008) 3035-3040.
[17] C. Pan, L. Dong, G. Zhu, S. Niu, R. Yu, Q. Yang, Y. Liu, Z. L. Wang, High-resolution electroluminescent imaging of pressure distribution using a piezoelectric nanowire LED array, Nature Photon, 7 (2013) 752-758.
[18] Y. Zhang, Y. Liu, Z. L. Wang, Fundamental Theory of Piezotronics, Adv. Mater., 23 (2011) 3004-3013.
[19] S. Zhang, B. Ma, X. Y. Zhou, Q. L. Hua, J. Gong, T. Liu, X. Cui, J. Y. Zhu, W. B. Guo, L. Jing, W. G. Hu, and Z. L. Wang. Strain-controlled power devices as inspired by human reflex, Nat Commun 11, 326 (2020).
[20] L. Zhu, Z. L. Wang, Progress in piezotronics and piezo-phototronics of quantum materials, J. Phys. D Appl. Phys., 52 (2019) 343001.
[21] M. Dan, G. Hu, L. Li, Y. Zhang, High performance piezotronic logic nanodevices based on GaN/InN/GaN topological insulator, Nano Energy, 50 (2018) 544-551.
[22] G. Hu, Y. Zhang, L. Li, Z. L. Wang, Piezotronic Transistor Based on Topological Insulators, ACS Nano, 12 (2018) 779-785.
[23] L. Zhu, Y. Zhang, P. Lin, Y. Wang, L. Yang, L. Chen, L. Wang, B. Chen, Z. L. Wang, Piezotronic Effect on Rashba Spin–Orbit Coupling in a ZnO/P3HT Nanowire Array Structure, ACS Nano, 12 (2018) 1811-1820.
[24] A. G. Swartz, P. M. Odenthal, Y. Hao, R. S. Ruoff, R. K. Kawakami, Integration of the Ferromagnetic Insulator EuO onto Graphene, ACS Nano, 6 (2012) 10063-10069.
[25] Z. Qiao, W. Ren, H. Chen, L. Bellaiche, Z. Zhang, A. H. Macdonald, Q. Niu, Quantum Anomalous Hall Effect in Graphene Proximity Coupled to an Antiferromagnetic Insulator, Phys. Rev. Lett., 112 (2014) 116404.
[26] Z. Wang, C. Tang, R. Sachs, Y. Barlas, J. Shi, Proximity-Induced Ferromagnetism in Graphene Revealed by the Anomalous Hall Effect, Phys. Rev. Lett., 114 (2015) 016603.
[27] G. B. Liu, W. Y. Shan, Y. Yao, W. Yao, D. Xiao, Three-band tight-binding model for monolayers of group-VIB transition metal dichalcogenides, Phys. Rev. B, 88 (2013) 085433.
[28] F. Zahid, L. Liu, Y. Zhu, J. Wang, H. Guo, A generic tight-binding model for monolayer, bilayer and bulk MoS_2, AIP Advances, 3 (2013) 052111.
[29] E. Cappelluti, R. Roldán, J. A. Silva-Guillén, P. Ordejón, F. Guinea, Tight-binding model and direct-gap/indirect-gap transition in single-layer and multilayer MoS_2, Phys. Rev. B, 88 (2013) 075409.
[30] H. Rostami, A. G. Moghaddam, R. Asgari, Effective lattice Hamiltonian for monolayer MoS_2: Tailoring electronic structure with perpendicular electric and magnetic fields, Phys. Rev. B, 88 (2013) 085440.
[31] H. Rostami, R. Asgari, Valley Zeeman effect and spin-valley polarized conductance in monolayer MoS_2 in a perpendicular magnetic field, Phys. Rev. B, 91 (2015) 075433.
[32] F. Khoeini, K. Shakouri, F. M. Peeters, Peculiar half-metallic state in zigzag nanoribbons of MoS_2: Spin filtering, Phys. Rev. B, 94 (2016) 125412.
[33] R. Roldán, M. P. López-Sancho, F. Guinea, E. Cappelluti, J. Á. Silva-Guillén, P. Ordejón, Momentum dependence of spin–orbit interaction effects in single-layer and multi-layer transition metal dichalcogenides, 2D Materials, 1 (2014) 034003.
[34] H. Rostami, R. Roldán, E. Cappelluti, R. Asgari, F. Guinea, Theory of strain in single-layer transition metal dichalcogenides, Phys. Rev. B, 92 (2015) 195402.

[35] W. A. Harrison, Elementary Electronic Structure: Revised, World Scientific Publishing Company, 1999.
[36] R. H. Liu, G. W. Hu, M. J. Dan, Y. M. Zhang, L. J. Li, and Y. Zhang, Piezotronic spin and valley transistors based on monolayer MoS_2, Nano Energy, 72 (2010) 104678.
[37] J. D. Jackson, Classical electrodynamics. 2007: John Wiley & Sons.
[38] K. A. N. Duerloo, M. T. Ong, E. J. Reed, Intrinsic Piezoelectricity in Two-Dimensional Materials, J. Phys. Chem. C, 3 (2012) 2871-2876.
[39] C. W. Groth, M. Wimmer, A. R. Akhmerov, X. Waintal, Kwant: a software package for quantum transport, New J. Phys., 16 (2014) 063065.
[40] D. Moldovan and F. M. Peeters, Pybinding v0.9.0: A Python Package for Tight-binding Calculations, http://dx.doi.org/10.5281/zenodo.56818.
[41] T. Ohta, A. Bostwick, T. Seyller, K. Horn, E. Rotenberg, Controlling the electronic structure of bilayer graphene, Science, 313 (2006) 951-954.
[42] J. B. Oostinga, H. B. Heersche, X. Liu, A. F. Morpurgo, L. M. Vandersypen, Gate-induced insulating state in bilayer graphene devices, Nature Mater, 7 (2008) 151-157.
[43] R. Roldán, A. Castellanos-Gomez, E. Cappelluti, F. Guinea, Strain engineering in semiconducting two-dimensional crystals, J. Phys.: Condens. Matter, 27 (2015) 313201.

Figure captions

Figure 1. (a) Schematic illustration of a MoS_2 ribbon. The red regions refer to the left and right leads. The number of atoms along the armchair edge *N* is used to describe the width of ZMDSN, which is indicated as *N*-ZMDSN. (b) and (d) show the direction of piezoelectric field under tensile and compressive strain, respectively. (c) Schematic illustration of the piezoelectric field in *N*-ZMDSN, where W is the width of the nonoribbon.

Figure 2. The band dispersion of a 21-ZMDSN with (a) no strain, (b) compressive strain $\varepsilon = -2\%$ and (c) tensile strain $\varepsilon = 5\%$. Band inversion in (a) and (b) indicates a negative gap.

Figure 3. (a) The band dispersion of 21-ZMDSN under tensile strain $(\varepsilon = 6.9\%)$ and exchange field $h=2.4\lambda_M$. Spin-up and spin-down region are labeled by red and blue colors. (b) Spin-dependent conductance and (c) spin polarization *p* as a function of the Fermi energy. Δ_s is the induced spin gap, in which full spin polarization can be achieved.

Figure. 4. (a) Energy dispersion of 21-ZMDSN under strain 6.9% with uniform piezoelectric field under various exchange field: (a) $\boldsymbol{h} = 1.075\boldsymbol{\lambda_M}$ and (b) $\boldsymbol{h} = 2.4\boldsymbol{\lambda_M}$. (c) Spin polarization $\boldsymbol{p}$ as a function of the Fermi energy.

Figure 5. Contour plot of the spin polarization *p* versus strain ε and Fermi energy E_F. At a fixed Fermi energy of -0.4 eV, three dots *A*, *B* and *C* correspond respectively to strain 6.6%, 7.6% and 8.6%, which is used in Fig. 5. Three critical strains (dashed line) are identified: $\varepsilon_1 = 3.6\%$, $\varepsilon_2 = 6.9\%$ and $\varepsilon_3 = 8.9\%$.

Figure 6. Energy dispersion of 21-ZMDSN under strain (a) 6.6%, (b) 7.6% and (c) 8.6%. (d) Corresponding electronic distribution at Fermi energy of -0.4 eV.

Figure 7. Schematic diagram of piezotronic spin transistor (a) without strain and (b) with tensile strain. Under tensile strain, spin polarized electrons travel through monolayer MoS_2 ribbon along the boundaries. Gate voltage is supplied to tune the Fermi level, and the gradient

color in MoS_2 ribbon labels the piezoelectric potential distribution.

Figure

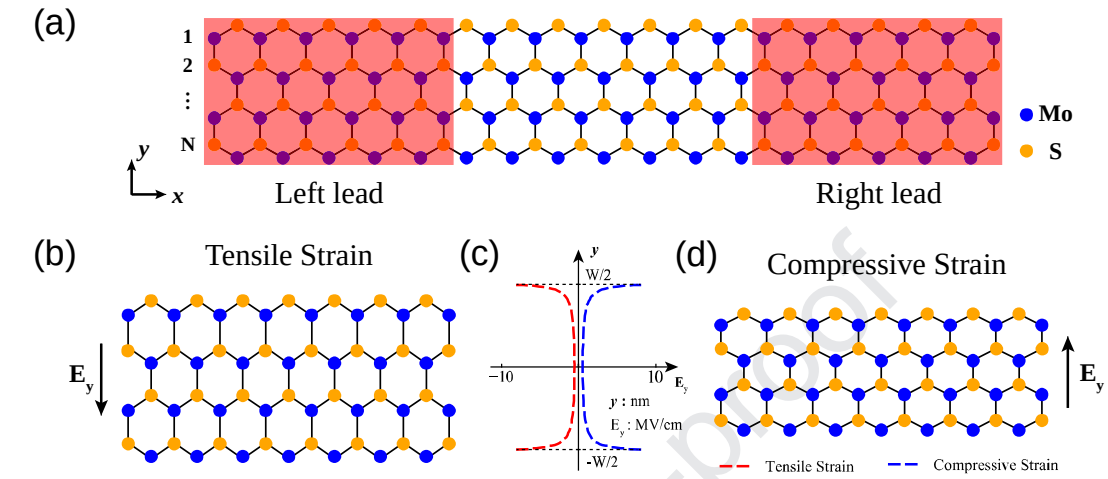

Fig 1

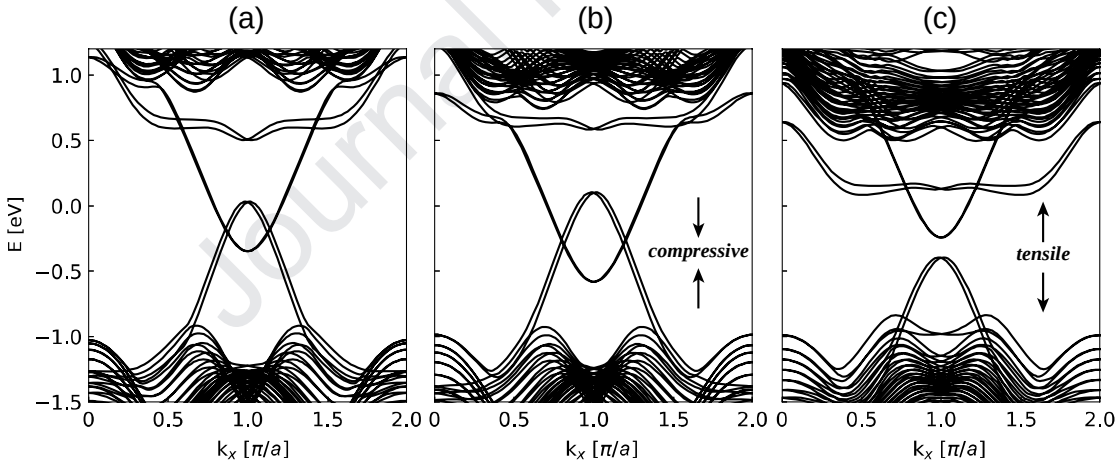

Fig 2

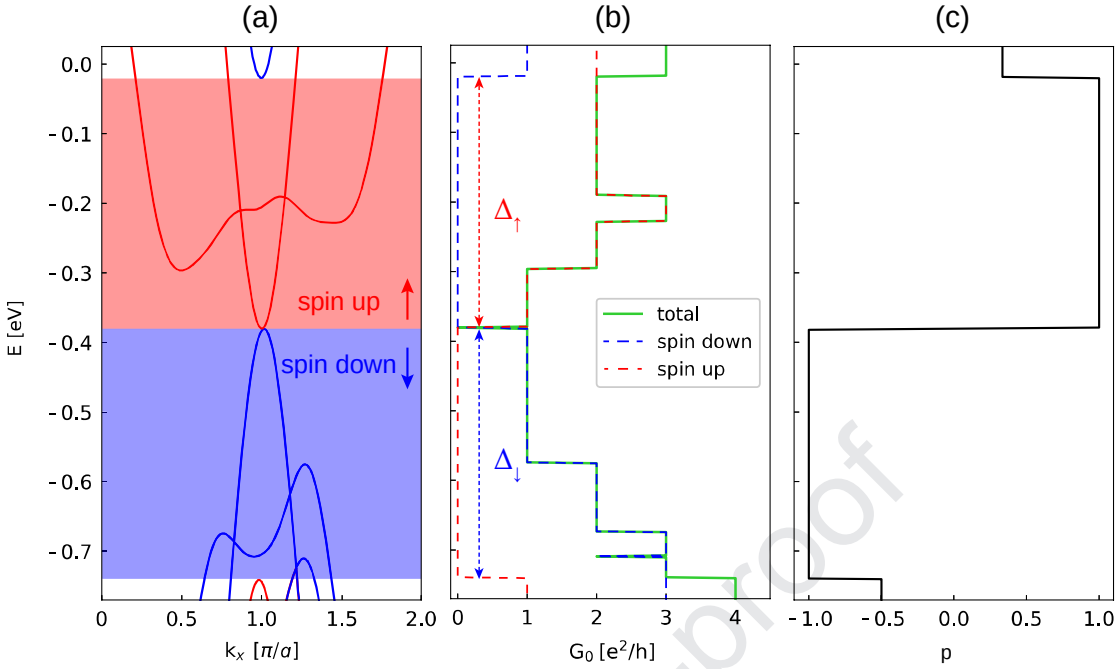

Fig 3

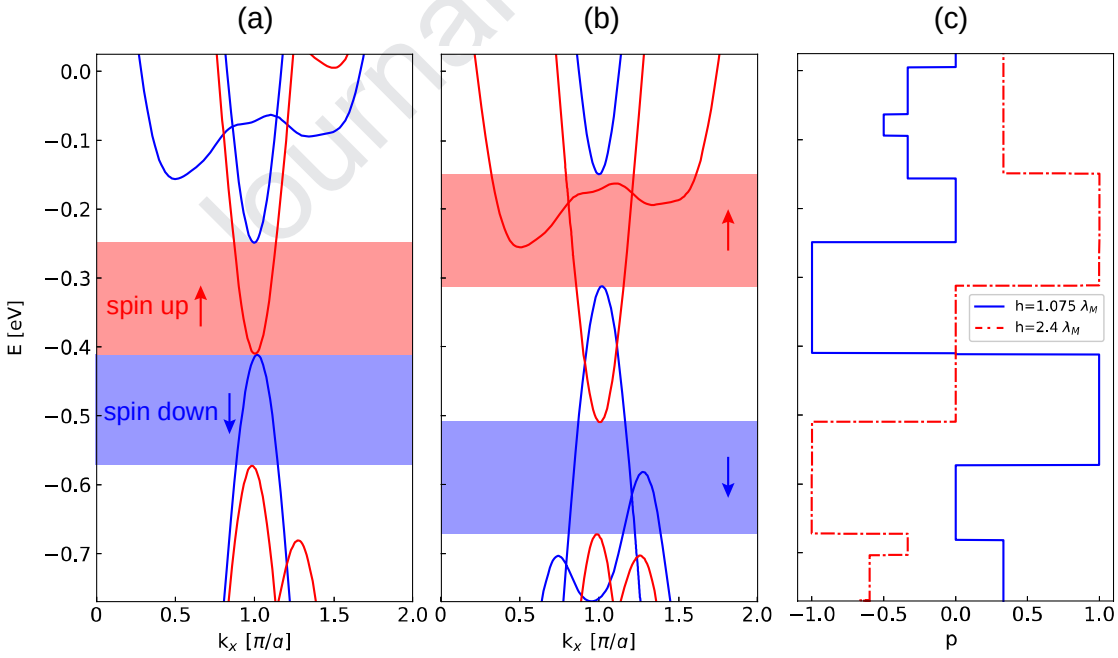

Fig 4

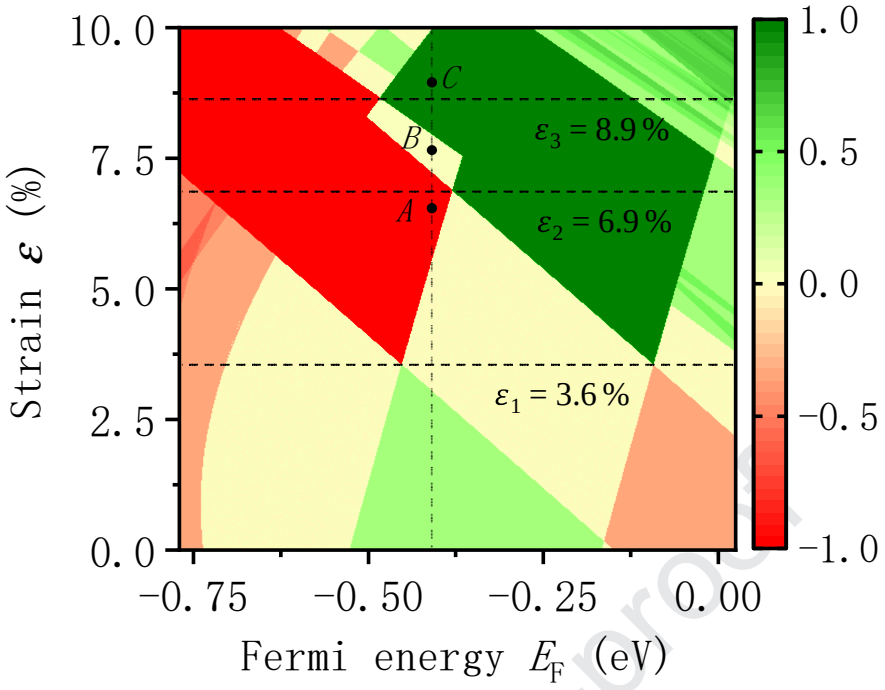
10.0
7.5
5.0
2.5
0.0
Strain ε (%)
−0.75
−0.50
−0.25
0.00
Fermi energy E_F (eV)
1.0
0.5
0.0
−0.5
−1.0
C
B
A
ε_3 = 8.9 %
ε_2 = 6.9 %
ε_1 = 3.6 %

Fig 5

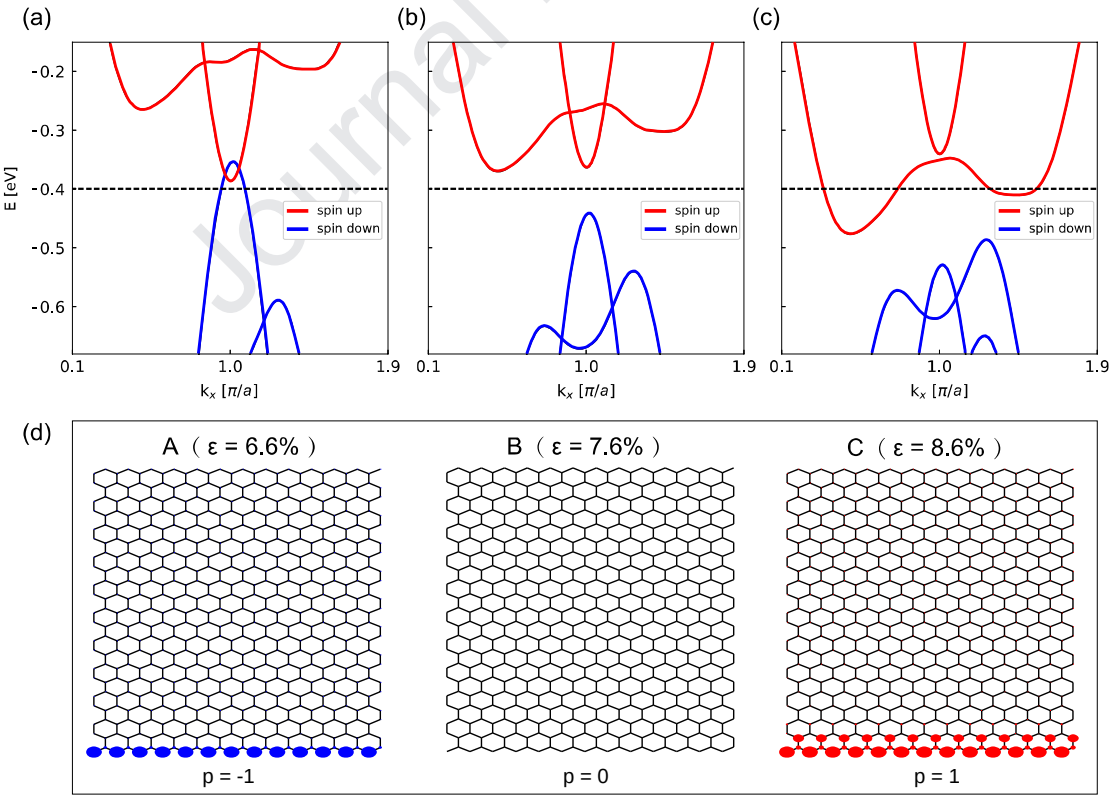
(a)
(b)
(c)
(d)
E [eV]
-0.2
-0.3
-0.4
-0.5
-0.6
0.1
1.0
1.9
k_x [π/a]
spin up
spin down
A （ ε = 6.6% ）
B （ ε = 7.6% ）
C （ ε = 8.6% ）
p = -1
p = 0
p = 1

Fig 6

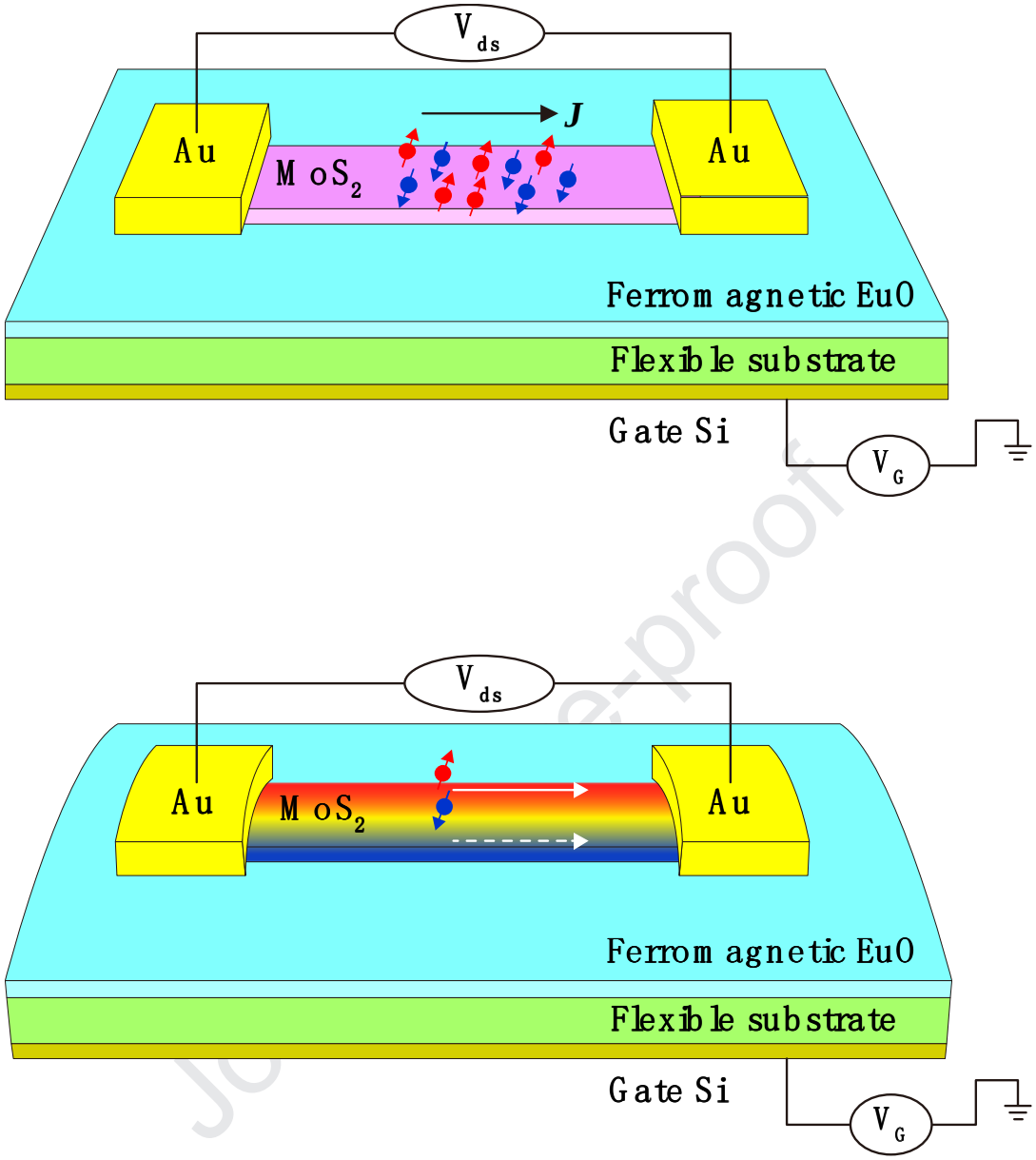
V ds
J
Au
M oS2
Au
Ferrom agnetic EuO
Flexible substrate
Gate Si
V G
V ds
Au
M oS2
Au
Ferrom agnetic EuO
Flexible substrate
Gate Si
V G

Fig 7

Xuefei Yan received his B. S. degree (2014) from Hunan Institute of Engineering. He is currently a M. S. student under the guidance of Professor Qiao Chen at Hunan Institute of Engineering. His research interests include electric structure and quantum transport in low dimensional systems.

Qiao Chen is a professor at Hunan Institute of Engineering, China. He received his B. S. degree (2004) from Hengyang Normal University and Ph. D degree (2009) in Condensed Matter Physics from Beijing Institute of Technology. His research interests include electronic structure and quantum transport in low dimensional systems.

Longlong Li is currently a postdoc researcher at University of Duisburg-Essen in Germany. His research interests include computational materials and physics using model Hamiltonian and density-functional approaches.

Huazhong Guo is an associate professor at Sichuan University, China. He received his B. S. degree (2003) from Hengyang Normal University and Ph. D degree (2008) in Condensed Matter Physics from Sichuan University. His research interests include electronic structure calculations from first-principles and quantum transport in mesoscopic systems.

Jinzhang Peng is a professor at Jishou University, China. He received his B. S. degree (1985) from Minzu University of China. His research interest includes physical properties of functional materials.

François Peeters is professor at the University of Antwerp (Belgium) and Yunnan University (China). He is Fellow of the European Physical Society, the American Physical Society, and he is member of the Royal Flemish Academy of Belgium and of the Academia Europea. His research involves theoretical modelling of the electronic, optical and magnetic properties of nanostructured semiconductors, superconductors, 2D atomic crystals (graphene, TMD, …) and hybrid systems.

Highlights:

1. The piezoelectric effect in MoS_2 nanoribbon induces a phase transition of edge states from metal to semiconductor.

2. In the presence of exchange field, edge states become semi-metallic with significant spin splitting and polarization that can be tuned by external strain.

3. By using a combination of external strain with exchange field to control the spin polarization of edge states, we showed that a 100% spin-polarized conductance is achieved both for spin-up and spin-down edge states over a wide range of strain magnitudes.